JACS
JOURNAL OF THE AMERICAN CHEMICAL SOCIETY
Article
pubs.acs.org/JACS

Gold–Copper Nanoalloys Supported on TiO_2 as Photocatalysts for CO_2 Reduction by Water

Ştefan Neaţu, Juan Antonio Maciá-Agulló, Patricia Concepción, and Hermenegildo Garcia*

Instituto Universitario de Tecnología Química CSIC-UPV, Universidad Politécnica de Valencia, Avda. de los Naranjos s/n, 46022, Valencia, Spain

Supporting Information

ABSTRACT: Commercial P25 modified by Au–Cu alloy nanoparticles as thin film exhibits, for CO_2 reduction by water under sun simulated light, a rate of methane production above 2000 μmol (g of photocatalyst)$^{-1}$ h^{-1}. Although evolution of hydrogen is observed and O_2 and ethane detected, the selectivity of conduction band electrons for methane formation is almost complete, about 97%. This photocatalytic behavior is completely different from that measured for Au/P25 (hydrogen evolution) and Cu/P25 (lower activity, but similar methane selectivity). Characterization by TEM, XPS, and UV–vis spectroscopy shows that Au and Cu are alloyed in the nanoparticles. FT-IR spectroscopy and chemical analysis have allowed one to detect on the photocatalyst surface the presence of $CO_2^{\bullet-}$, Cu–CO, and elemental C. Accordingly, a mechanism in which the role of Au is to respond under visible light and Cu binds to CO and directs the reduction pathway is proposed.

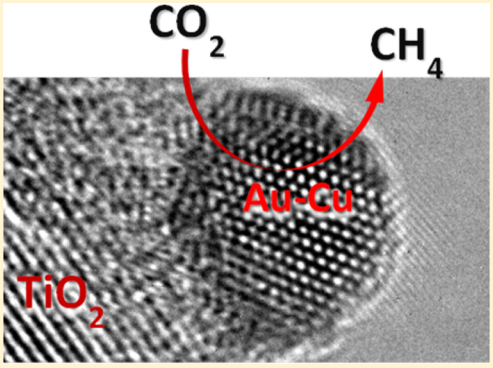

INTRODUCTION

Reduction of carbon dioxide to useful chemicals is receiving considerable attention as a long-term alternative to the depletion of fossil fuels as well as a mean to valorize CO_2 emissions. As chemical reduction of CO_2 by water is energetically uphill, this process must consume energy, preferably from renewable resources. The photocatalytic CO_2 reduction by water as reducing agent, reported for the first time more than three decade ago,[1,2] is gaining increasing interest considering it could be carried out using sunlight as the primary energy source. There are a large number of studies on CO_2 photoreduction, and a wide variety of materials, especially semiconductors employed for water splitting into H_2 and O_2, have been evaluated for this purpose.[3−8] Among the various semiconductors, titania has been the most frequently employed photocatalyst due to a number of advantages including abundance, low-cost, low-toxicity, high UV photoactivity, and chemical and thermal stability.[9−11]

Although titania is the most studied semiconductor in the field of photocatalysis, both for water splitting and for CO_2 reduction, its efficiency is still far from optimum due to the lack of visible-light photoresponse and the large percentage of unwanted electron–hole recombination of the photogenerated charge separated state that reduces considerably the quantum efficiency of the process.

One of the main issues associated with the photocatalytic CO_2 reduction by H_2O over titania is the hydrogen formation as a preferential or competitive process, limiting the overall CO_2 reduction yields and affecting the selectivity of the reaction mixture. Generally hydrogen is formed in much higher yield than the total amount of products derived from CO_2 reduction.[12] At this moment, the best strategy to limit the dominant hydrogen production prevailing over photocatalytic CO_2 reduction is the use of suitable cocatalysts to modify the selectivity of TiO_2. The use of cocatalysts has opened in recent years the possibility to control TiO_2 photoactivity toward CO_2 reduction.[11] The presence of noble metals such as Pt, Au, Ag, or Cu on TiO_2 has an enhancing effect over CO_2 conversion to valuable hydrocarbons.[3−16] Simultaneously to the use of cocatalysts, an additional viable methodology that has been used to enhance the efficiency of titania is nanostructuring of the photocatalyst with defined particle morphology.[17,18] Despite the advances in this field, at present only few studies have exploited the wide range of possibilities that binary combinations of metals offer as cocatalysts in photocatalytic CO_2 reduction.[17−20] It has been reported that the presence of platinum and copper cocatalysts on TiO_2 increases the efficiency of the photocatalytic CO_2 reduction, leading mainly to methane with a good selectivity.[17−20]

Continuing with this approach, herein we report the notable increase in the photocatalytic efficiency and selectivity to methane of TiO_2 as photocatalyst for CO_2 reduction by H_2O upon deposition on the photocatalyst surface of both gold and copper nanoparticles (NPs). Au and Cu loaded on titania renders a material that, under visible light irradiation and optimal conditions, results in methane formation rates of about 2.2 ± 0.3 mmol g^{-1} h^{-1} equivalent to 10.67 ± 0.1 mmol m^{-2} h^{-1} and selectivity of electrons toward methane generation of 97%.

Received: July 2, 2014
Published: October 20, 2014

   dx.doi.org/10.1021/ja506433k | J. Am. Chem. Soc. 2014, 136, 15969–15976

EXPERIMENTAL SECTION

Photocatalysts Preparation. Gold and copper loaded titania photocatalysts were prepared by the stepwise deposition−precipitation of each metal.[21,22] First, the gold loaded titania materials were obtained by adding the titania support (1 g) to a 100 cm^3 aqueous solution of $HAuCl_4$ (containing from 10 to 20 mg of $HAuCl_4{\cdot}3H_2O$) previously adjusted at pH ≈ 8.5 with a NaOH solution (0.2 M). The slurry was maintained at 75 °C, under vigorous stirring. Heating the slurry in the deposition step reduces the time required in this process to 5 h. After this time, the sample was filtered and washed with deionized water until the complete removal of chloride using $AgNO_3$ test. Au−TiO_2 then was dried under vacuum at 80 °C for 48 h and calcined at 400 °C in air for 2 h with a heating rate of 1.25 °C min^{-1}. The obtained Au/TiO_2 powders were added to a 100 cm^3 aqueous solution of $Cu(NO_3)_2$ (containing from 38 to 19 mg of $Cu(NO_3)_2{\cdot}3H_2O$) previously adjusted at pH ≈ 8.5 with a NaOH solution (0.2 M) and stirred at 75 °C for 5 h. The solids were recovered by filtration, washed thoroughly with deionized water, and dried under vacuum at 80 °C. The TiO_2 powders containing Au and Cu were reduced under H_2 flow (80 mL × min^{-1}) at 400 °C for 2 h with a heating rate of 1.25 °C min^{-1}. For the photocatalytic tests, small amounts of (Au, Cu)−TiO_2 powders were dispersed by ultrasonication in Milli-Q water and deposited as a thin layer over quartz plates with an area of 1.25 cm^2 using the spray technique. The weight of the deposited photocatalyst was determined by weighting the plates (about 50 mg) before and once dried after spraying (estimated error 0.2 mg) and also by determining the thickness of the layer by means of an optical profilometer (1 nm resolution, 1.5 μm thickness) and multiplying the volume of the layer by TiO_2 P25 density (3.8 g/cm^3). Supporting Information Figure S1 provides some microscopy images and the measurement of the thickness for one of these films.

Photocatalysts Characterization. All of the photocatalysts have been investigated by means of optical (UV−vis in DR mode) and vibrational (FT-IR) spectroscopy. Other characterization techniques, like elemental analysis, transmission electron microscopy, and X-ray photoelectron spectroscopy, have been used to investigate the composition and the structure of these materials. The experimental details are presented in the Supporting Information.

Photocatalytic Test. The irradiation of CO_2/H_2O mixture was carried out by powder or by thin layer of the photocatalyst deposited on 1.25 cm^2 (1 × 1.25 cm × cm rectangle) quartz plates placed in the center of an aluminum tray located inside the photoreactor perpendicular to the light beam. Compressed CO_2 (99.995%, Linde Spain) regulated by a mass flow controller was passed at room temperature through a water bubbler to generate CO_2 and H_2O vapor mixture. The gas mixture was then flushed through a rectangular photoreactor (300 mL internal volume) with aluminum walls and Pyrex window. The reactor has the size of 200 mm (length) × 80 mm (width) × 55 mm (height) and was located 10 cm below the solar simulator beam outlet. After being purged for 1 h, the gas valves on both sides were closed to seal the reactor, and the CO_2 pressure was typically regulated to 1.7 atm. Irradiation with simulated sunlight of the photocatalyst films was carried out using an Oriel solar simulator (with a 1000 W Xe lamp) coupled with an AM1.5 filter that provides simulated concentrated sunlight (1000 mW cm^{-2}, see Supporting Information Figure S1d for the lamp emission spectrum that contains about 4% UV light and http://assets.newport.com/webDocuments-EN/images/12298.pdf for a more complete description of the equipment used). During the irradiation, the temperature increased from the ambient value to a maximum of 60 °C measured at the aluminum tray, and the pressure in the chamber reaching 1.9 atm at this temperature. To determine the influence of irradiation type (UV vs vis), two independent reactions have been performed using the most active (Au, Cu)/TiO_2 material. Two different types of irradiation sources, either a 125 W high-pressure Hg lamp from Philips in the case of UV experiments, or a 150 W Xe lamp from Hamamatsu with a UV cutoff filter (>400 nm) in the case of visible light experiments, were used. Experiments comprising the use of photocatalysts thin films with different surface areas have been performed. To this purpose, the most active material has been deposited on quartz plates having 1, 3, and 6 cm^2 surface area. The course of the reaction was followed by analyzing periodically the gas phase. At the final time, the possibility that elemental carbon or organic compounds could be present adsorbed onto the photocatalyst films was also considered, and the photocatalytic materials were submitted to combustion chemical analysis and solid−liquid extraction using dichloromethane as the solvent. No products were detected in the extract. Reproducibility of the data was checked by performing independent experiments in duplicate, whereby consistent results with significantly low dispersions (<5%) were obtained. During the irradiation period, the gaseous samples in the reactor were taken at desired intervals by directly coupling one of the photoreactor valves to a dual-channel gas chromatograph (Agilent Technology 490 Micro GC) equipped with MS5A and PPQ columns and two TCDs. To double-check the reproducibility of the data, a second Rapid Refinery Gas Analyzer from Bruker that consists of a three-channel gas chromatograph has been used. The first channel with a TCD detector performed H_2 analysis by using a micropacket HayeSep Q and Molsieve 5 Å column with Ar as carrier gas. At the second channel equipped with another TCD detector, CO_2, CO, O_2, and N_2 could be analyzed with a combination of micropacket HayeSep Q, H−N, and Molsieve 13 columns with He as carrier gas. The last channel analyzes C1−C5 hydrocarbons with He as carrier gas and a FID detector. The calibration data obtained with the two GC systems were similar to variation smaller than 5%. Calibration was made by injecting mixtures of CO_2, CH_4, or H_2 in N_2 with known proportions. The data are automatically processed by software of the instruments that provide concentration data even when GC is connected directly to the photoreactor. GC measurements were also performed in a blank control using a mixture of ultrahigh purity argon (instead of CO_2) and water vapor as the purging and reaction gas, respectively, for the catalyst-loaded reactor; no carbon-containing compounds were detected derived from the photocatalyst upon irradiation. This verifies that the methane observed in our experiments is not an artifact due to contamination of organic residues on the photocatalyst. A series of other control tests were also conducted using a mixture of CO_2 and H_2O vapor as the purging and reaction gas, respectively, for both the empty reactor and the aluminum tray in the photoreactor. Again, for either case, no carbon-containing compounds were produced under irradiation. This demonstrates that the reactor and the tray were clean and that the CO_2 conversion cannot proceed without the photocatalyst. All of these background tests have proved that any carbon-containing compounds produced must be originated from CO_2 through photocatalytic reactions.

RESULTS AND DISCUSSION

Photocatalytic Conversion of CO_2 with H_2O. The procedure used in the preparation of TiO_2 modified by Au and Cu NPs has been already sufficiently documented.[20−26] The simultaneous presence of NPs of two metals acting as cocatalysts on TiO_2 should lead to new optical, electronic, and catalytic properties that are different from those of their monometallic counterparts, and these new properties could be reflected in the enhancement of the activity and selectivity in the CO_2 reduction by water.[27,28] Although the activity of both metals individually loaded on titania has been already reported for CO_2 reduction, the use of their combination has been so far scarcely studied.[20,29]

To investigate the influence of the combination of Au−Cu NPs on the photocatalytic activity, a series of (Au, Cu)/TiO_2 samples, containing a constant total metal amount of 1.5 wt % and Au/Cu ratios varying from 1:2 to 2:1, were synthesized and compared for the CO_2 reduction to the performance of pure 1.5 wt % Au- and Cu-loaded TiO_2 as reference samples. Au and Cu NPs were loaded on Evonik P25 TiO_2 by using two consecutive deposition steps. First, Au loaded on TiO_2 material is prepared by adding TiO_2 support to an $AuCl_4^-$ solution

dx.doi.org/10.1021/ja506433k | J. Am. Chem. Soc. 2014, 136, 15969−15976

previously adjusted to pH 8.5 performing the deposition in 5 h by heating at 75 °C. After several steps of filtration, washing, and drying, the resulting powder is thermally treated in air at 400 °C for 2 h to obtain Au/TiO_2. This intermediate Au/TiO_2 was used in a second deposition of Cu from aqueous solution using $Cu(NO_3)_2$ as precursor. The obtained TiO_2 powder is subjected to a thermal reducing step with H_2 at 400 °C for 2 h, affording (Au, Cu)/TiO_2 photocatalyst as dark purple solid. Before its use as photocatalyst, (Au, Cu)/TiO_2 was always submitted to H_2 reduction. Control samples Au/TiO_2 and Cu/TiO_2 were prepared by deposition of a single metal precursor.

The photocatalytic activity of TiO_2-based materials for reduction of CO_2 by H_2O was determined in the gas phase under batch conditions. H_2 and CH_4 were the only two major products that have been observed in this work in all of the experiments. It should be noted that using (Au, Cu)/TiO_2 as photocatalysts, no CO could be observed in the gas phase even after 46 h irradiation, and just a small amount of oxygen and ethane was detected. Ethane appears as a secondary product derived from methane. The temporal evolution of H_2 and CH_4 production toward 46 h of irradiation using the most active material is presented in Supporting Information Figure S1. The linearity in the CH_4 and H_2 production indicates that the photocatalyst is extremely stable, the photocatalytic activity starting to decay when enough O_2 is formed, probably due to the quenching of photogenerated electrons by this gas. Table 1 summarizes the H_2 and CH_4 production rates in $\mu mol \times g^{-1} \times h^{-1}$ for the series of photocatalysts under study. As it can be seen there, (Au, Cu)/TiO_2 (Au/Cu 1:2) was the most efficient photocatalyst, probably due to the optimal atomic composition of Au versus Cu. The role of Au introducing visible light photoresponse and that of Cu directing the selectivity toward CO_2 reduction could be responsible for the existence of this optimal composition, as it will be discussed below. Table 1 also contains the selectivity of photogenerated electrons toward CO_2 reduction and the selectivity of CH_4 versus H_2 (numbers in brackets in the central column of Table 1). Considering that the splitting of H_2O to H_2 is competitive with the reduction of CO_2 to CH_4, the selectivity for CO_2 reduction on an electron basis (8 e^- for the formation of CH_4 and 2 e^- in the case of H_2 production) has been calculated using the following equation:[26]

$$\text{selectivity} = [8n(CH_4)]/[8n(CH_4) + 2n(H_2)] \times 100\%$$

where $n(CH_4)$ and $n(H_2)$ are the number of moles of CH_4 and H_2 formed at a given time.

To firmly prove the photocatalytic CO_2 conversion, we have performed several control experiments, including (i) contacting for long periods CO_2 and H_2O with the catalyst in the dark, (ii) simulated solar light irradiation in the absence of catalyst, and (iii) irradiation of the catalyst with simulated sunlight in argon atmosphere instead of CO_2 and H_2O gas mixture. Analysis of the gas phase in these three controls did not lead to the detection of any reaction product, including the lack of observation of H_2 and CH_4. This indicates that the reduction of CO_2 and H_2O is a photocatalytic process. These controls also show that H_2 and CH_4 do not arise from inorganic or organic residues that could be adsorbed on the photocatalyst surface.

The CO_2 photoreduction process was initially performed using the photocatalyst as powders on an aluminum tray. Under these conditions, TiO_2 presents almost no activity, and the presence of both metallic cocatalysts on TiO_2 leads to a significant increase of the photoactivity and selectivity, but still far from the performance when using these photocatalysts as thin films (see Table 1). Because the photocatalytic reaction takes place only on the surface of the materials, the next logical step was to perform the reaction using the correct quantity of solid material until the optimal value of methane generation rate is reached. This can be accomplished by using thin micrometric films keeping constant the irradiated area. In our case, the optimal value for having the highest value in terms of photoactivity and selectivity was 0.6 mg of solid material deposited on photocatalytically inert quartz plates having an area of 1.25 cm^2. This optimization of the amount of photocatalyst by depositing them as thin films leads to a notable increase of methane evolution rate as a consequence of the optimization of the weight of photocatalyst to the material that is exposed to the light (see Supporting Information Figure S1).

The data presented in Table 1 show that the photocatalysts as thin films can exhibit very high photocatalytic efficiency. It can be seen that Au−Cu catalysts exhibit much higher activity than TiO_2 (about 50 times) for both monometallic counterparts (about 1 order of magnitude). In particular, monometallic Au catalyst possesses higher activity for H_2 production and lower selectivity for CO_2 reduction as compared to the Cu/TiO_2. The bimetallic system produces the largest amount of CH_4, which is nearly 8−11 times that obtained with both monometallic Cu or Au loaded TiO_2 materials, respectively. The increase in the amount of Cu in the Au−Cu system enhances both the activity and the selectivity. As it can be seen in Table 1, the best performing photocatalytic material of the (Au, Cu)/TiO_2 series is the one having a Au/Cu ratio of 1:2. This influence of the composition of the metal nanoparticles on the photocatalytic activity is not totally unexpected considering that previous related studies in the literature have reported that the selectivity of the CO_2 photoreduction is determined by the chemical composition of the photocatalyst.[18,19] In this regard, it has been observed that hydrocarbons are preferentially formed

Table 1. Photocatalytic Reduction of CO_2 by H_2O in the Gas Phase over TiO_2 Loaded with Single or Binary Metal Cocatalysts under Simulated Sunlight[a]

photocatalyst	selectivity for CO_2 reduction (%)	formation rate (μmol g^{-1} h^{-1})	
		H_2	CH_4
	Powders[b]		
TiO_2	0 (0)[c]	2	0
Au/TiO_2[b]	79 (48.5)	34	32
(Au, Cu)/TiO_2 (Au/Cu 2:1)	87 (62.7)	19	32
(Au, Cu)/TiO_2 (Au/Cu 1:1)	89 (66.7)	16	32
(Au, Cu)/TiO_2 (Au/Cu 1:2)	92 (73.3)	16	44
Cu/TiO_2	91 (71.4)	16	40
	Films[d]		
TiO_2	80 (50)	48	50 ± 7
Au/TiO_2	94 (80.8)	49	210 ± 30
(Au, Cu)/TiO_2 (Au/Cu 1:2)	97 (88.6)	286	2200 ± 300
Cu/TiO_2	97 (89.4)	33	280 ± 80

[a]Reaction conditions: feed, 1.7 atm water-saturated CO_2; irradiation time, 6 h; photocatalyst, 1.25 cm^2 thin film (0.6 mg of solid material) deposited on quartz plates. [b]50 mg of solid material. [c]The numbers in brackets indicate the selectivity of CH_4 as reaction product calculated by dividing the numbers of moles of CH_4 by the total amount of moles generated during the photocatalytic process (CH_4 plus H_2). [d]Estimated relative error ±15% (see the Supporting Information).

dx.doi.org/10.1021/ja506433k | J. Am. Chem. Soc. 2014, 136, 15969−15976

on Cu-containing TiO_2, while CO was formed on Au containing photocatalysts.[11] The data presented in Table 1 indicate that the simultaneous presence of Au and Cu in appropriate proportion enhances considerably the activity of Cu/TiO_2 preserving the selectivity in CH_4 formation.

Table 2 presents the photocatalytic results obtained upon irradiation of three surface areas of (Au, Cu)/TiO_2 (Au/Cu 1:2) films on quartz plate. In principle, a constant formation rate and CH_4 selectivity should be observed in the area value range under study. However, data of Table 2 show a certain improvement of the performances of the photocatalyst as the surface area increases. This apparent positive trend could be due to the difficulty in the preparation by spray pyrolysis of films with exactly the same mass per substrate surface area as the dimensions of the surface increases. In any case, the data of Table 2 show that the excellent performance of (Au, Cu)/TiO_2 films extends for areas higher than 1.25 cm^2, that is, the area value of the data presented in Table 1.

Table 2. Photocatalytic Reduction of CO_2 by H_2O in the Gas Phase over (Au, Cu)/TiO_2 (Au/Cu 1:2) Thin Films with Different Surface Areas under Simulated Sunlight[a]

photocatalyst	surface area (cm^2)	CH_4 productivity (μmol m^{-2} h^{-1})[b]	selectivity for CO_2 reduction (%)
(Au, Cu)/TiO_2 (Au/Cu 1:2)	1	550 ± 11	83.3
	3	640 ± 13	92.7
	6	660 ± 13	93.5

[a]Reaction conditions: feed, 1.7 atm water-saturated CO_2; irradiation time, 6 h; 150 W, Xe lamp; photocatalyst, thin films deposited on quartz plates. [b]Estimated relative error 2% (see the Supporting Information)

Because in this study both metals are present in the chemical composition of the photocatalyst, one point of interest is to determine the distribution of the two metals in (Au, Cu)/TiO_2 to understand the origin of the activity and selectivity of these photocatalysts. This issue was studied by transmission electron microscopy and XPS technique.

Surface Characterization of (Au, Cu)/TiO_2 Solids. TEM studies were performed to evaluate the composition, structure, and distribution of the NPs within the photocatalysts matrix. TEM images show mainly round-shaped NPs with an average size of around 5 nm. This average particle size is similar to that of Au NPs of the (Au, Cu)/TiO_2 sample before H_2 reduction (see Figure S3 in the Supporting Information). The *d*-spacing values measured on different nanoparticles were found to be in the range of 0.195−0.235 nm. In the case of (Au, Cu)/TiO_2 (Au/Cu ratio 1:2), we found peaks at 0.235 nm (Au (111) JCPDS 04-0784), 0.208 nm (Cu (111) JCPDS 04-0836), 0.222 nm (AuCu (111) JCPDS 25-1220, CuAu (1 10 1) JCPDS 27-0156, and Cu_3Au_2 (1 11 1) JCPDS 27-0157), and 0.195 (AuCu (200) JCPDS 25-1220, CuAu (200) JCPDS -27-0156, and Cu_3Au_2 (1 19 0) JCPDS 27-0157). These *d* measurements indicate that (Au, Cu)/TiO_2 material is constituted by Au−Cu alloy NPs, together with independent Au and Cu NPs. Figure 1 presents the HRTEM image of a representative Au−Cu alloy NP, which possesses a *d*-spacing value of 0.222 nm. The composition of the Au−Cu nanoparticles was determined by dispersive X-ray spectroscopy. For this purpose, different nanoparticles were analyzed, and the profile spectra were taken. The corresponding EDS patterns (see Supporting Information Figure S2) confirmed the presence of both Au and Cu in the same NPs, in agreement with the presence of Au−Cu alloy on TiO_2. Quantitative EDS analysis of the NPs provides an average Au/Cu atomic ratio of 75:25, while the presence of unalloyed Cu NPs in the material could be also detected (see Supporting Information Figure S3). These observations clearly show that the (Au, Cu)/TiO_2 photocatalyst presents a distribution of the Au−Cu alloy NPs together with the coexistence of unalloyed gold and copper NPs. Quantitative determination of the distribution of Au−Cu composition would require a statistical analysis of a large

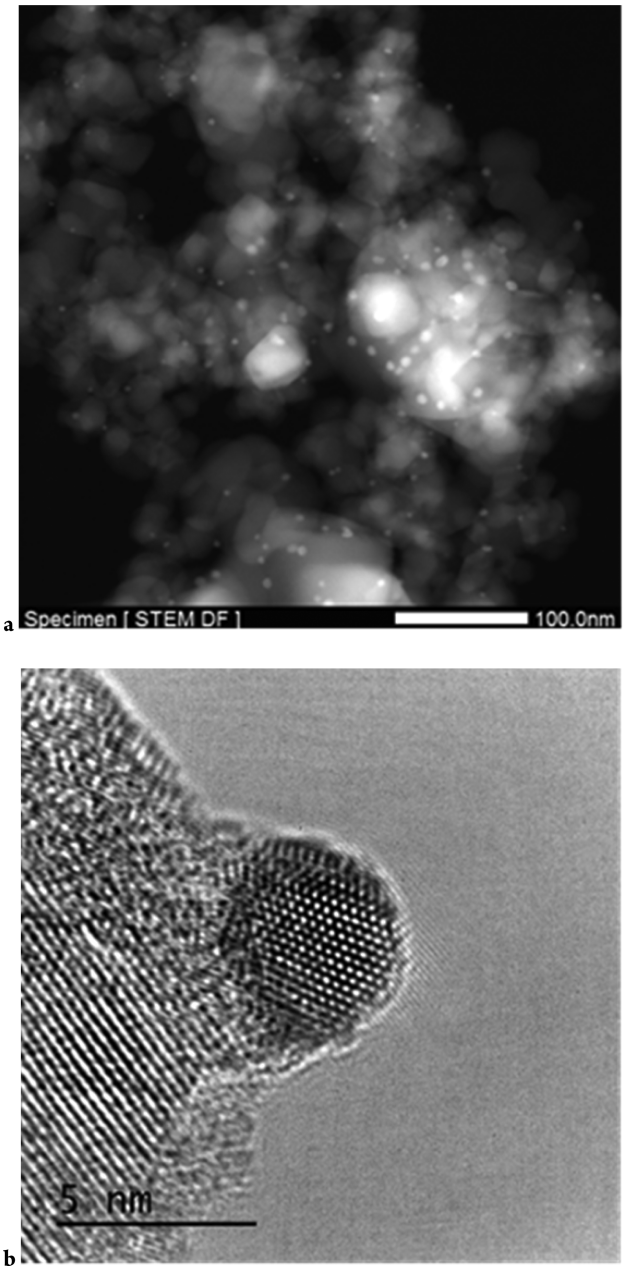

Figure 1. Structure analysis of the most active photocatalyst. (a) Transmission electron microscopy (TEM) images of (Au, Cu)/TiO_2 (Au/Cu ratio 1:2) after Au−Cu alloy formation at 400 °C in H_2 atmosphere. (b) High-resolution TEM (HRTEM) image of one Au−Cu alloy nanoparticle with a *d*-spacing value of 0.222 nm that is different from that of independent Au (0.235 nm) or Cu (0.208 nm) NPs.

dx.doi.org/10.1021/ja506433k | J. Am. Chem. Soc. 2014, 136, 15969−15976

number of particles and consideration of their corresponding diameters that is out of the scope of the present study.

It should be noted, however, that the photocatalytic stability of (Au, Cu)/TiO_2 materials suggests that Au−Cu alloy NPs are tolerant to the redox stress of the mechanism. Thus, in view of the presence of Au−Cu alloy NPs in (Au, Cu)/TiO_2 and the contrasting behavior of this photocatalyst with respect to Au/TiO_2 and Cu/TiO_2, it is reasonable to attribute the good photocatalytic performance of (Au, Cu)/TiO_2 to the properties of Au−Cu alloy NPs that exhibit selectivity similar to that of Cu/TiO_2 and higher photoresponse.

To understand the reasons of enhanced CH_4 production in the photocatalytic reduction of CO_2 by H_2O on (Au, Cu)/TiO_2 catalysts, the samples were also characterized by UV−vis spectroscopy in diffuse reflectance (DR) mode. The DR-UV−vis spectra of the (Au, Cu)/TiO_2 sample before and after the reduction in H_2 atmosphere are presented in Figure 2.

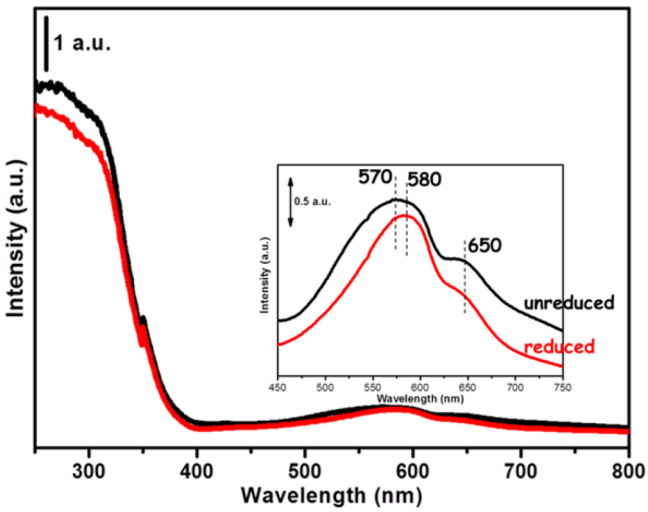

Figure 2. UV−vis analysis of the most active photocatalyst. The DR-UV−vis spectra of the (Au, Cu)/TiO_2 (Au/Cu ratio 1:2) catalyst before and after reduction at 400 °C in H_2 atmosphere. The inset presents the red-shift of the plasmonic band of Au NPs after the reduction process. The shift in the position of the plasmon band indicates the formation of the Au−Cu alloy NPs, and the decrease in the 650 nm band corresponding to Cu^{2+} ions is related to their reduction to Cu^0 and incorporation in the alloy.

As it can be observed, besides the typical absorption band with onset 390 nm corresponding to the electronic interband transition in TiO_2 (optical band gap 3.2 eV), the spectra of (Au, Cu)/TiO_2 samples before the reductive H_2 treatment at 400 °C exhibit a clear band centered at around 570 nm assigned to the surface plasmon absorption of Au NPs and an optical absorption located at 650 nm attributable to the presence of Cu. During the thermal treatment in H_2 atmosphere, the d−d transitions significantly decrease because the Cu ions undergo reduction and alloy with Au NPs. Simultaneously, the plasmonic band of Au NPs appears to be red-shifted to around 580 nm. This behavior might be an indication that Au and Cu start to form nanoalloys.[30,31]

XPS data of the (Au, Cu)/TiO_2 (Au/Cu ratio 1:2) sample reveal that the Au, Cu surface composition changes after hydrogen reduction (Cu/Au atomic ratio 10.6 in the fresh sample while 4.5 in the reduced samples and 12.16 after photocatalytic reaction), indicative of gold segregation toward the particle surface (see Supporting Information Table S1). The Cu/Au ratio higher than 2 for the unreduced (Au, Cu)/TiO_2 (Au/Cu 1:2) could be a reflection of the preparation procedure in which the metals are deposited consecutively, first Au and then Cu. Therefore, it seems that Cu is preferentially located more externally than Au. Subsequently, reduction under H_2 at 400 °C should lead to the formation of metal alloy NPs where the proportion of Au on the external surface is more similar to the value of the bulk chemical analysis. Upon the use of (Au, Cu)/TiO_2 (Au/Cu 1:2) as photocatalyst, XPS shows again a Cu concentration on the external surface similar to that of the unreduced material. All of these variations indicate metal atom mobility on the surface of TiO_2 and restructuring of the metal NPs. Similar surface restructuring, already reported for nanoalloys,[32] suggests that both metals should be in close contact instead of forming individual particles. The in situ hydrogen reduced (Au, Cu)/TiO_2 sample shows a binding energy of 83.5 eV for Au $4f_{7/2}$, which is consistent with the Au^0 oxidation state, and a binding energy of 931.8 eV for Cu $2p_{3/2}$ (associated with Cu^0) with a slight shoulder at 933.4 eV (associated with Cu^{2+}) (see Supporting Information Figure S4). The lower binding energy of the Cu $2p_{3/2}$ XPS peak for the reduced (Au, Cu)/TiO_2 sample (931.8 eV) relative to the expected value for bulk Cu (which is 932.7 eV) could be related to some electronic and/or final state effect due to Au−Cu nanoalloy formation.[33] Moreover, Auger parameter analysis agrees with a different local state of the copper atoms in the (Au, Cu)/TiO_2 sample relative to a bulk copper metal sample (see the Supporting Information). To have a clearer image of the photocatalysts behavior, several low-temperature CO adsorption in situ FT-IR experiments have been performed. Indeed, nanoalloy formation is also confirmed from FT-IR studies of CO adsorption (see Supporting Information).

Interesting, following the CO_2 photoreduction, the sample exhibited a new component in the C 1s XPS peak at ca. 290 eV, suggesting that some carbonaceous residues were accumulated on the catalyst. These deposits of carbon residues may be intermediates in the reduction of CO_2 to CH_4 (see Supporting Information Figure S5). It is also important to mention that the carbon content of the materials after performing the photocatalytic reaction has been determined by elemental chemical analysis and is estimated to be around 0.21%.

Mechanism for Photocatalytic CO_2 Reduction. In situ FTIR spectroscopy has proved to be a powerful technique to gain understanding on the mechanism and reaction intermediates in photocatalysis.[34] In the present case, compressed self-supporting pellets suitable for IR spectroscopy were used.

All IR spectra recorded for (Au, Cu)/TiO_2 (Au/Cu ratio 1:2) exhibit a sharp intense band at 3735 cm^{-1} due to stretching vibration of the isolated (noninteracting) surface OH groups, accompanied by a broad band in the low frequency side due to OH groups forming hydrogen bridges bonded to Ti^{4+} species, and a well-defined band at 3717 cm^{-1}, which has been assigned to the presence of Ti^{3+}−OH based on the literature.[35] The generation of Ti^{3+} sites is not totally unexpected after the thermal treatment under H_2 atmosphere at 400 °C (see Figure 3a), although its population has to be sufficiently low to be undetectable by XPS. The bands located at 3430 and 1635 cm^{-1}, respectively, are assigned to the OH stretching and bending vibration of water, which in the case of reduced sample are slightly pronounced (see Figure 3a). The exposure to 185 mbar CO_2 and 190 mbar of water leads to the appearance of two bands located at 2350 and 2342 cm^{-1} due to the presence

dx.doi.org/10.1021/ja506433k | J. Am. Chem. Soc. 2014, 136, 15969−15976

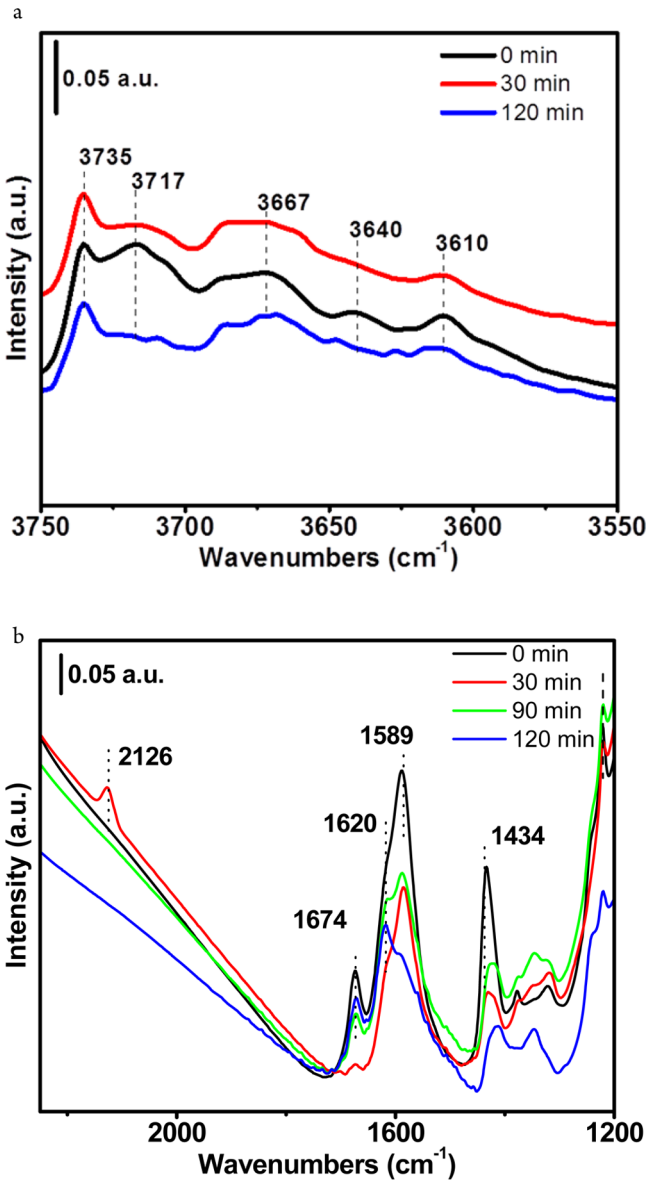

Figure 3. Infrared spectroscopic analysis of the surface bound intermediates generated during CO_2 and H_2O adsorption and their evolution upon irradiation: (a) In situ FTIR spectra in the 3750−3550 cm^{-1} region before (black spectrum) and after (red and blue spectra) adsorption of CO_2 on (Au, Cu)/TiO_2 (Au/Cu ratio 1:2). (b) In situ FTIR spectra in the 2250−1150 cm^{-1} region before (black spectrum) and after 30, 90, and 120 min of irradiation of the (Au, Cu)/TiO_2 (Au/Cu ratio 1:2).

of CO_2 in the gas phase, and the presence of other bands due to the generation of carbonate/carboxylate species by interaction with (Au, Cu)/TiO_2 photocatalyst (Figure 3b). Specifically, new IR bands at 1589, 1378, 1323 cm^{-1}; 1620, 1434, 1221 cm^{-1}; and 1674, 1243 cm^{-1} were observed. The IR bands at 1620, 1434, 1221 cm^{-1} are assigned to bicarbonate HCO_3^- species in addition to the IR band at 3610 cm^{-1} (see Figure 3a) based on the agreement with the literature.[36−43] However, assignment of the IR bands at 1674 and 1589 cm^{-1} to either carboxylate or carbonate like species is not straightforward, due to the ambiguity found in literature data.[36−44] From the IR spectra of CO_2 adsorption of a (Au, Cu)/TiO_2 sample purposely oxidized at 300 °C under O_2 atm (see Supporting Information Figure S10), where no Ti^{3+} should be expected, and the in situ time-resolved IR spectra taken during irradiation (see Figure 3b and discussion below), we can attribute the IR band at 1589 cm^{-1} to a carboxylate $CO_2^{\bullet-}$ like species, while the IR band at higher frequency 1674 cm^{-1} should be related to a carbonate $CO_3^{=}$ like species. Similar assignment has been observed in previous literature data.[40−44]

The spectroscopic detection of $Ti^{4+}-CO_2^{\bullet-}$ suggests that CO_2 can be activated by specific Ti^{3+} sites possessing an excess of electron density respect to Ti^{4+}. Ti^{3+} species would be formed by reductive thermal annealing with H_2. These electron-rich Ti^{3+} will transfer spontaneously an electron to surface adsorbed CO_2 leading to $CO_2^{\bullet-}$. In good agreement with the proposal for the generation of $CO_2^{\bullet-}$, Figure 3a shows that the band associated with OH groups bonded to Ti^{3+} sites appearing at 3717 cm^{-1} is constantly decreasing and eventually disappears after the interaction of (Au, Cu)/TiO_2 with CO_2. The generation of HCO_3^- and $CO_3^{=}$ species is expected to be caused by the direct coordination of CO_2 with basic $Ti^{4+}-OH$ and $Ti^{4+}-O^{2-}$ groups, respectively.

The in situ time-resolved IR spectra taken during irradiation presented in Figure 3b show that after 30 min UV irradiation all peaks at 1674, 1589, 1433, and 1243 cm^{-1} decrease in intensity. These decreases in intensity could be related to a thermal effect due to irradiation (see Supporting Information Figure S11) and/or a catalytic effect. The growth of the Cu−CO band at 2126 cm^{-1} upon 30 min irradiation agrees with a photocatalytic effect (CO_2 photoreduction by water). From the first spectrum, it is difficult to identify which IR bands are the precursors of CO formation. However, when following the time evolution of the IR spectra during irradiation (see Figure 3b), regeneration of the IR bands at 1674, 1620 cm^{-1} is observed, while only the band at 1589 cm^{-1} clearly decreases in intensity. According to this result, we assign the 1589 cm^{-1} IR band as the reactive species, being the precursor of CO. The fact that Cu^+-CO is not more observed in the IR spectra could be due to consecutive reaction of Cu^+-CO to CH_4 and/or to a low stability of the Cu^+-CO complex upon increasing irradiation time (see Supporting Information Figure S12). Thus, we have evidence supporting $CO_2^{\bullet-}$ as the intermediate species, with the IR band at 1589 cm^{-1} being the precursor of CO formation. Note that in the experiments performed in the photoreactor there is an excess of CO_2 that ensures the continued, constant formation of CH_4 during the whole irradiation period, while in the IR experiments the amount of CO_2fnew IR bands at 1589, 1378, 1323 becomes depleted. Also note that no CO was detected in the gas phase in the experiments using the photoreactor. Overall, these spectroscopic data confirm that CO_2 is photocatalytically reduced to CO due to the presence of Ti^{3+}, and that surface bound $CO_2^{\bullet-}$ species is one of the most likely reaction intermediates in the reduction of CO_2 on (Au, Cu)/TiO_2. The process can take place to some extent even in the dark if the (Au, Cu)/TiO_2 photocatalyst is previously submitted to reductive treatment.

These spectroscopic data regarding the nature of the surface bound intermediates generated by CO_2 adsorption and their evolution upon irradiation provided by in situ FTIR and XPS techniques (detection of elemental C on the photocatalyst surface) give some hints on the photoreduction mechanism.

To gain further insights into the activity of (Au, Cu)/TiO_2, two sets of irradiations were performed using filtered UV or visible light. To prove that the visible light activity is imparted by the Au plasmonic effect, two other experiments comprising the use of bare TiO_2 and Cu/TiO_2 under visible light

dx.doi.org/10.1021/ja506433k | J. Am. Chem. Soc. 2014, 136, 15969−15976

irradiation have been performed. After exposing (Au, Cu)/TiO_2 (Au/Cu 1:2) powder (25 mg) for 24 h to these two irradiations with different wavelengths, interesting important variations in the product selectivity were obtained. Analysis of the product distribution reveals that CH_4 is only formed under visible light exposure (21.47 μmol g^{-1}), while H_2 generation is observed in different amounts upon irradiation in both wavelength ranges (22.19 μmol g^{-1} under UV and 7.74 μmol g^{-1} under visible light irradiation). This difference in product selectivity is remarkable and can be rationalized on the basis of precedents reporting the visible light photocatalytic activity of titania containing Au NPs and the influence of the excitation wavelength.[45−47] When the photocatalyst is irradiated with UV light, direct TiO_2 excitation with wavelengths shorter than 380 nm leads to charge separation on the semiconductor, followed by electron migration to the metal NPs. In this case, Au−Cu alloy NPs will act as electron reservoir and cocatalyst transferring electrons mainly to water or acting as charge electron−hole recombination centers. When a visible light irradiation source is used, Au NPs act as light harvester due to their surface plasmon band in the visible light. A similar proposal of specific visible light excitation of Au NPs and UV light excitation of TiO_2 on a Au−TiO_2 sample has been used to explain photocatalytic thiol oxidation to disulfide under visible light and disulfide to thiol reduction upon UV irradiation using Au−TiO_2 as photocatalyst.[47] This specific visible response due to the presence of Au NPs also agrees with the present study because the experiments performed by using bare TiO_2 and Cu/TiO_2 show that these materials do not present photocatalytic activity under visible light irradiation. Hot electrons from Au are mainly transferred to oxidized surface Cu atoms rather to the conduction band of TiO_2,[26] while the excess of holes oxidizes water and generates protons. The surface activated CO_2 molecules (mainly on Cu sites) start to be reduced, and the generation of CH_4 begins to occur. When the irradiation source comprises the entire solar light spectrum, both UV and visible-light induced processes take place simultaneously in various degrees; in this way, the enhancement of the H_2 and CH_4 generation is observed due to the presence of noble metal NPs. The different roles of Au−Cu NPs depending on the excitation wavelength and distinctive location of electrons and holes are summarized in Figure 4.

With respect to the route of CH_4 formation, the CO_2 photoreduction mechanism in the presence of water starts with the adsorption of both reactants, CO_2 and H_2O, leading to the formation of a distribution of adsorbed species, followed by their activation by one-electron and one-hole transfer, respectively. After the activation of CO_2 by a one-electron transfer and formation of surface-bonded $CO_2^{\bullet-}$, the reduction proceeds through a series of elementary steps involving the consecutive transfer of protons and electrons, resulting in the cleavage the C−O bonds being substituted by new C−H bonds. Some intermediates, particularly $CO_2^{\bullet-}$, Cu−CO, and carbon deposits on the surface, have been successfully detected. The overall schematic mechanism of the gas-phase CO_2 photoreduction with H_2O over (Au, Cu)/TiO_2 materials apparently follows the so-called "carbene pathway" that has been proposed earlier[11] (see Figure 4).

CONCLUSIONS

The data presented show that Au- and Cu-loaded TiO_2 photocatalyst in the appropriate Au/Cu ratio is an extremely efficient material for the solar-light reduction of CO_2 to CH_4, with H_2O as reducing agent exhibiting a production rate of 2.2 ± 0.3 mmol g^{-1} h^{-1}. Under optimal conditions, selectivity value of photogenerated electrons toward the reduction of CO_2 of 97% was observed with minimal concomitant H_2 generation. The origin of the photocatalytic activity seems to be the Au−Cu alloy NPs. These results constitute another example showing very selective materials for photocatalytic production of CH_4 at very high conversion based on the combination in the adequate proportions of two or more metals acting as cocatalysts of TiO_2 semiconductor, managing electrons and controlling the selectivity of the process. It appears that the selectivity toward CH_4 formation arises from the presence of Cu bonding to CO on the photocatalyst, while the visible light photoresponse would be introduced by the surface plasmon band of Au.

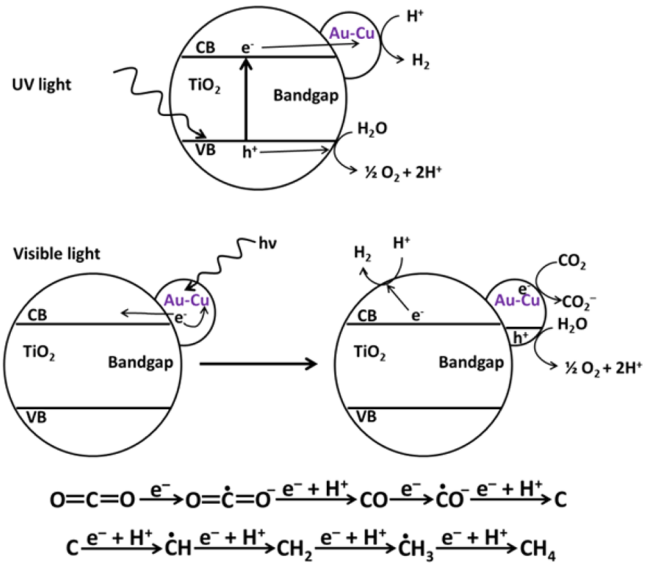

Figure 4. Top part summarizes the proposal to rationalize the influence of the irradiation wavelength range on the product distribution using (Au, Cu)/TiO_2 as photocatalysts. The bottom part presents a plausible route for methane generation in the gas-phase CO_2 photoreduction by water.

ASSOCIATED CONTENT

Supporting Information

Experimental procedures, TEM images, low-temperature FT-IR carbon monoxide adsorption experiments, and supplementary in situ FT-IR spectra. This material is available free of charge via the Internet at http://pubs.acs.org.

AUTHOR INFORMATION

Corresponding Author

hgarcia@qim.upv.es

Notes

The authors declare no competing financial interest.

ACKNOWLEDGMENTS

This work has been supported by the Marie Curie project PIEF-GA-2011-298740. Financial support by the Spanish Ministry of Economy and Competitiveness (Severo Ochoa CTQ 2012-32315) and the Generalidad Valenciana (Prometeo 2012/2013) is gratefully acknowledged. J.A.M.-A. acknowledges the assistance of the CSIC for their award of a Postdoctoral JAE-Doc contract.

REFERENCES

(1) Halmann, M. *Nature* **1978**, *275*, 115−116.
(2) Inoue, T.; Fujishima, A.; Konishi, S.; Honda, K. *Nature* **1979**, *277*, 637−638.
(3) Indrakanti, V. P.; Kubickib, J. D.; Schobert, H. H. *Energy Environ. Sci.* **2009**, *2*, 745−758.
(4) Roy, S. C.; Varghese, O. K.; Paulose, M.; Grimes, C. A. *ACS Nano* **2010**, *4*, 1259−1278.
(5) Dhakshinamoorthy, A.; Navalon, S.; Corma, A.; Garcia, H. *Energy Environ. Sci.* **2012**, *5*, 9217−9233.
(6) Mori, K.; Yamashita, H.; Anpo, M. *RSC Adv.* **2012**, *2*, 3165−3172.
(7) Navalon, S.; Dhakshinamoorthy, A.; Alvaro, M.; Garcia, H. *ChemSusChem* **2013**, *6*, 562−577.
(8) Izumi, Y. *Coord. Chem. Rev.* **2013**, *257*, 171−186.
(9) Chen, X.; Mao, S. S. *Chem. Rev.* **2007**, *107*, 2891−2959.
(10) Kubacka, A.; Fernandez-Garcia, M.; Colon, G. *Chem. Rev.* **2012**, *112*, 1555−1614.
(11) Habisreutinger, S. N.; Schmidt-Mende, L.; Stolarczyk, J. K. *Angew. Chem., Int. Ed.* **2013**, *52*, 7372−7408.
(12) Neatu, S.; Macia-Agullo, J. A.; Garcia, H. *Int. J. Mol. Sci.* **2014**, *15*, 5246−5262.
(13) Feng, X.; Sloppy, J. D.; LaTempa, T. J.; Paulose, M.; Komarneni, S.; Bao, N.; Grimes, C. A. *J. Mater. Chem.* **2011**, *21*, 13429−13433.
(14) Wang, W. N.; An, W. J.; Ramalingam, B.; Mukherjee, S.; Niedzwiedzki, D. M.; Gangopadhyay, S.; Biswas, P. *J. Am. Chem. Soc.* **2012**, *134*, 11276−11281.
(15) In, S. I.; Vaughn, D. D., II; Schaak, R. E. *Angew. Chem., Int. Ed.* **2012**, *51*, 3915−3918.
(16) Xie, S.; Wang, Y.; Zhang, Q.; Fan, W.; Deng, W.; Wang, Y. *Chem. Commun.* **2013**, *49*, 2451−2453.
(17) Varghese, O. K.; Paulose, M.; LaTempa, T. J.; Grimes, C. A. *Nano Lett.* **2009**, *9*, 731−737.
(18) Zhang, X.; Han, F.; Shi, B.; Farsinezhad, S.; Dechaine, G. P.; Shankar, K. *Angew. Chem., Int. Ed.* **2012**, *51*, 12732−12735.
(19) Zhai, Q.; Xie, S.; Fan, W.; Zhang, Q.; Wang, Y.; Deng, W.; Wang, Y. *Angew. Chem., Int. Ed.* **2013**, *52*, 5776−5779.
(20) Ovcharov, M. L.; Shvalagin, V. V.; Granchak, V. M. *Theor. Exp. Chem.* **2014**, *50*, 53−58.
(21) Shiraishi, Y.; Takeda, Y.; Sugano, Y.; Ichikawa, S.; Tanaka, S.; Hirai, T. *Chem. Commun.* **2011**, *47*, 7863−7865.
(22) Tsukamoto, D.; Shiro, A.; Shiraishi, Y.; Sugano, Y.; Ichikawa, S.; Tanaka, S.; Hirai, T. *ACS Catal.* **2012**, *2*, 599−603.
(23) Lim, B.; Jiang, M. J.; Camargo, P. H. C.; Cho, E. C.; Tao, J.; Lu, X. M.; Zhu, Y. M.; Xia, Y. N. *Science* **2009**, *324*, 1302.
(24) Powers, D. C.; Ritter, T. *Nat. Chem.* **2009**, *1*, 302.
(25) Tao, F.; Grass, M. E.; Zhang, Y. W.; Butcher, D. R.; Renzas, J. R.; Liu, Z.; Chung, J. Y.; Mun, B. S.; Salmeron, M.; Somorjai, G. A. *Science* **2008**, *322*, 932.
(26) Sugano, Y.; Shiraishi, Y.; Tsukamoto, D.; Ichikawa, S.; Tanaka, S.; Hirai, T. *Angew. Chem., Int. Ed.* **2013**, *52*, 5295−5299.
(27) Chaudhuri, R. G.; Paria, S. *Chem. Rev.* **2012**, *112*, 2373−2433.
(28) Liu, S.; Sun, Z.; Liu, Q.; Wu, L.; Huang, Y.; Yao, T.; Zhang, J.; Hu, T.; Ge, M.; Hu, F.; Xie, Z.; Pan, G.; Wei, S. *ACS Nano* **2014**, *8*, 1886−1892.
(29) Hou, W.; Hung, W. H.; Pavaskar, P.; Goeppert, A.; Aykol, M.; Cronin, S. B. *ACS Catal.* **2011**, *1*, 929−936.
(30) Pramanik, S.; Kr Mishra, M.; De, G. *CrystEngComm* **2014**, *16*, 56−63.
(31) Motl, N. E.; Ewusi-Annan, E.; Sines, I. T.; Jensen, L.; Schaak, R. E. *J. Phys. Chem. C* **2010**, *114*, 19263−19269.
(32) Alayoglu, S.; Tao, F.; Altoe, V.; Specht, C.; Zhu, Z.; Aksoy, F.; Butcher, D. R.; Renzas, R. J.; Liu, Z.; Somorjai, G. A. *Catal. Lett.* **2011**, *141*, 633−640.
(33) Liorca, J.; Dominguez, M.; Ledesma, C.; Chimentao, R. J.; Medina, F.; Sueiras, J.; Angurell, I.; Seco, M.; Rossell, O. *J. Catal.* **2008**, *258*, 187−198.
(34) Neatu, S.; Parvulescu, V. I.; Epure, G.; Petrea, N.; Somoghi, V.; Ricchiardi, G.; Bordiga, S.; Zecchina, A. *Appl. Catal., B* **2009**, *91*, 546−553.
(35) Wu, W.; Bhattacharyya, K.; Gray, K.; Weitz, E. *J. Phys. Chem. C* **2013**, *117*, 20643−20655.
(36) Baltrusaitis, J.; Schuttlefield, J.; Zzeitler, E.; Grassian, V. H. *Chem. Eng. J.* **2011**, *170*, 471−481.
(37) Liu, L.; Zhao, C.; Li, Y. *J. Phys. Chem. C* **2012**, *116*, 7904−7912.
(38) Yang, C. C.; Hu, Y. H.; van der Linden, B.; Wu, J. C. S.; Mul, G. *J. Am. Chem. Soc.* **2010**, *132*, 8398−8406.
(39) Su, W. G.; Zhang, J.; Feng, Z. C.; Chen, T.; Ying, P.; Li, C. *J. Phys. Chem. C* **2008**, *112*, 7710−7716.
(40) Busca, G.; Lorrencelli, V. *Mater. Chem.* **1982**, *7*, 89.
(41) Kiselev, V. F.; Krylov, O. V. In *Springer Series in Surface Science*; Ertl, G., Gomer, R., Eds.; Springer-Verlag: Berlin, 1989; Vol. *9*.
(42) Turek, A. M.; Wachs, I. E.; Canio, E. D. *J. Phys. Chem.* **1992**, *96*, 5000−5007.
(43) Martra, G. *Appl. Catal., A* **2000**, *200*, 275−285.
(44) Collins, S. E.; Baltanas, M. A.; Bonivardi, A. L. *J. Phys. Chem. B* **2006**, *110*, 5498.
(45) Primo, A.; Corma, A.; Garcia, H. *Phys. Chem. Chem. Phys.* **2011**, *13*, 886−910.
(46) Primo, A.; Marino, T.; Corma, A.; Molinari, R.; Garcia, H. *J. Am. Chem. Soc.* **2011**, *133*, 6930−6933.
(47) Naya, S.-i.; Teranishi, M.; Isobe, T.; Tada, H. *Chem. Commun.* **2010**, *46*, 815−817.